

Research Article

# NUMERICAL SIMULATION OF THERMO-FLUID DYNAMIC ENTROPY GENERATION IN CENTRIFUGAL COMPRESSORS FOR MICRO-TURBINE APPLICATION

**K. Wasinarom**  
**D. Boonchauy**  
**J. Charoensuk\***  
Department of Mechanical Engineering, Faculty of Engineering, King Mongkut's Institute of Technology Ladkrabang, Bangkok, Thailand 10520

## ABSTRACT:

The investigation on quantitative entropy generation in the streamwise direction of flow passage in centrifugal compressors with different exit beta angle was carried out under the operating condition of small gas turbine application. The flow field was obtained by 3D numerical simulation with the help of commercial CFD code. The analysis coupled both flow structure and quantitative entropy generated from the inlet through to outlet. The comparison has been made among 10°, 20°, 30°, 40° and 50° exit beta angle. The simulation result showed that at the streamwise location of 0.1-0.6, entropy generated around 60 J/kgK per streamwise location length for all exit beta angles, where the inflow direction was parallel with the inlet impeller passage. In contrast to the location of 0.6-1.0, the entropy generated around 480 J/kgK per streamwise location length, around 8 times of the entropy generated in location 0.1-0.6. This was correspondent to high deformation rate of the flow field in this area. The separation and secondary flow can be observed as a result of blade tip flow leakage. Moreover, strong flow distortion with massive turbulent intensity took place, and as a consequence, high local eddy viscosity was present. Increasing the beta angle had alleviated jet-wake shear layer at the exit area of the compressor as a consequence of less entropy generation in the location of 0.6-1.0 streamwise location.

**Keywords:** Entropy, flow passage, centrifugal compressor

## 1. INTRODUCTION

Micro-turbine engine (MT) become more practical means of power generation. This application has several advantages compared to reciprocating engine. MT has more capability to operate with wider range of low calorific fuel. Because MT has continuous combustion process. MT has better combustion efficiency and less emission. Although, MT compression ratio is limited by turbine inlet temperature (TIT) and components efficiency. Nowadays, compressor efficiency and turbine inlet temperature are increasing with the help of CFD and material technology. Consequently, higher compression ratio and thermal efficiency of small gas turbine engine can be realized. Moreover, exhaust temperature of gas turbine is generally higher than reciprocating engine, which increase the potential to recover waste heat from the exhaust gas.

\* Corresponding author: J. Charoensuk  
E-mail address: kcjaruw@kmitl.ac.th



Thermal efficiency of small gas turbine depends on the operation of three engine's sub-components which comprised of 1.) Compressor 2.) Combustion chamber 3.) Turbine. In order to achieve high system thermal efficiency, each component have to operate with high efficiency at their operating condition. The operating condition of individual sub-component can be obtained from thermodynamics analysis. Thermodynamics analysis is working on the working fluid state at the inlet and outlet of the engine sub-component in order to analyst on the system operation performance. Thermodynamics analysis is the engineering tool which is able to carry out sub-component's desired working fluid state, during initial design phase. It is able to analyst on coupled interaction of sub-component efficiency and the restriction of firing temperature of turbine. It shows that a small gas turbine engine, with compressor has an efficiency of 78% (including combustor pressure drop), turbine firing temperature at 1200K, is able to achieve thermal efficiency at around 28% (Fig 1) which comparable to piston engine. The recuperative cycle micro-gas turbine application is considered as high potential for commercial application. MT engine is able to integrate in co-generation or tri-generation system with interesting profitability potential in Thailand. Many available Micro-turbine manufacturers select recuperative cycle for their designed engine. Most of them provide engine's thermal efficiency around 30% with optimum pressure ratio around 4. At this low pressure ratio condition, the compressor is possible to employ single stage centrifugal compressor which is considered as a benefit for low manufacturing capital cost of the MT. Moreover, MT integrate with synthesis gas from gasifier (BIG/GT) reactor, is currently become the most interesting research topic due to their advantage compare with reciprocating engine. MT is capable to consume hot synthesis gas from the gasifier reactor at around 500 °C. At this temperature, tar is in vapor stage. So it could directly burn in turbine combustor. In contrast to reciprocating engine which synthesis gas is necessary to cool down to room temperature while all tar need to remove before deliver syn-gas to engine. Therefore, Micro-turbine is considered to deliver higher system thermal efficiency with gasification reactor integration.

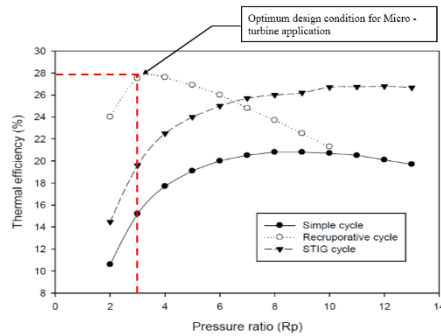


Fig. 1. Thermal efficiency of small gas turbine.

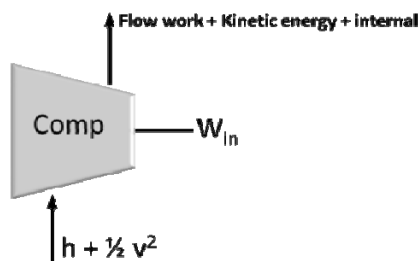


Fig. 2. Compressor Energy analysis.

Entropy generation is the quantitative parameter. It indicates the reversibility of process where energy is transformed from useful pressure and kinetics form to useless thermal internal energy (Fig. 2). The transformed energy is dissipated in working fluid. Thermodynamics discipline is categorized dissipation process as the internal irreversibility. Increasing in dissipation relates to increasing in input energy required to obtain target exit pressure and flow rate. Local entropy generation depends on local internal flow structure. Entropy generation in compressor and turbine has significant impact on system thermal efficiency [1]. It is generally cast by isentropic efficiency. In order to design compressor that capable to operate with high isentropic efficiency at design condition, physical flow field that occur in the flow passage have to be well understood. Flow field characteristic is a result of

various interaction. Despite two third of entropy was generated in the diffuser [2], it has been studied that diffuser efficiency was largely dependent on impeller exit flow condition. The interaction at the transition area from impeller to diffuser inlet significantly contribute to the overall a compressor performance [3]. However, flow in diffuser is beyond the scope of discussion in this paper.

## 2. GOVERNING EQUATIONS

3-D Reynolds averaged compressible Navier-Stokes equations was used for governing equations. The transport of momentum, mass, energy are taken into account. Eddy viscosity was computed by  $k$ - $\varepsilon$  turbulent modeling. Mass and momentum transport equation can be written as below

$$\frac{\partial}{\partial x_i} (\rho u_i) = 0 \quad (1)$$

$$\frac{\partial}{\partial x_j} (\rho u_i u_j) = -\frac{\partial P}{\partial x_i} + \frac{\partial}{\partial x_j} \left[ \mu \left( \frac{\partial u_i}{\partial x_j} + \frac{\partial u_j}{\partial x_i} - \frac{2}{3} \delta_{ij} \frac{\partial u_l}{\partial x_l} \right) \right] + \frac{\partial}{\partial x_j} \left[ \mu \left( \frac{\partial u_i}{\partial x_j} + \frac{\partial u_j}{\partial x_i} \right) - \frac{2}{3} \left( \rho k + \mu_t \frac{\partial u_l}{\partial x_l} \right) \delta_{ij} \right] \quad (2)$$

The local entropy generation depends on mean flow velocity gradient and level of turbulent intensity which can be computed via the equation below.

TKE transport and TKE dissipation transport can be computed using the transport equation below

$$\frac{\partial}{\partial t} (\rho k) + \frac{\partial}{\partial x_i} (\rho k u_i) = \frac{\partial}{\partial x_j} \left[ \left( \mu + \frac{\mu_t}{\sigma_k} \right) \frac{\partial k}{\partial x_j} \right] + P_k - \rho \varepsilon \quad (3)$$

$$\frac{\partial}{\partial t} (\rho \varepsilon) + \frac{\partial}{\partial x_i} (\rho \varepsilon u_i) = \frac{\partial}{\partial x_j} \left[ \left( \mu + \frac{\mu_t}{\sigma_\varepsilon} \right) \frac{\partial \varepsilon}{\partial x_j} \right] + C_{\varepsilon 1} \frac{\varepsilon}{k} G_k - C_{\varepsilon 2} \rho \frac{\varepsilon^2}{k} \quad (4)$$

When  $\sigma_k$  and  $\sigma_\varepsilon$  are the turbulent Prandtl numbers assigned to be constants equal to 1.0 and 1.3 respectively,  $P_k$  is the local turbulent generation rate which is proportional to local mean flow velocity gradient, can be computed by the equation below

$$P_k = \left[ \mu_t \left( \frac{\partial u_i}{\partial x_j} + \frac{\partial u_j}{\partial x_i} \right) - \frac{2}{3} \left( \rho k + 3 \mu_t \frac{\partial u_l}{\partial x_l} \right) \delta_{ij} \right] \frac{\partial u_j}{\partial x_i} \quad (5)$$

Turbulent viscosity ( $\mu_t$ ) can be calculated using assumption for  $k$ - $\varepsilon$  turbulent modeling which depends on local values of TKE and TKE dissipation rate as below

$$\mu_t = \rho C_\mu \frac{k^2}{\varepsilon} \quad (5)$$

Where  $C_{\varepsilon 1}$ ,  $C_{\varepsilon 2}$  and  $C_\mu$  are assigned to be 1.44, 1.92 and 0.09 respectively.

## 3. BOUNDARY CONDITIONS AND NUMERICAL METHODOLOGY

Preliminary compressor geometry was obtained corresponding to the designed thermodynamics cycle for 200 kW rated power gas turbines application (Table 1, [16]). The preliminary design procedure conducted on thermodynamics analysis that detailed flow was not considered and attention was given on state of working fluid at the inlet and outlet of the engine sub-component [4, 5]. After that, CFD was implemented for flow analysis.

Detailed geometry and fine tuning of the flow passage were made in order to achieve high isentropic efficiency and desired operating condition.

**Table 1:** Thermodynamics data

Isentropic Efficiency of Compressor	85
Pressure Ratio	4
Mass flow rate (kg/s)	1.33

**Table 2:** Geometry dimension from [9-11]

Dimension	Size
Inlet impeller diameter (mm)	90
Outlet impeller diameter (mm)	440
Inlet impeller height (mm)	15
Outlet impeller height (mm)	10
Number of impeller / splitter blade	9/9
Impeller speed (rpm)	20,000
Tip clearance (mm) [8]	1

### 3.1 Numerical methodology

The computational study has been conducted by commercial ANSYS CFX Code [15]. The flow had been modeled with RANS scheme.  $k-\varepsilon$  Turbulent model was employed to predict transport of turbulent property. Governing equation was discretized by Finite volume method. Flow domain was divided into 630,000 cells of structured hexahedral cell [6, 8, 14]. Grid independent was tested by compressor model of previous research [6, 7]. High grid density was employed in near wall region to capture high gradient of flow property in that area. The normalized residual convergence criteria of every transport equation was set at  $1.0^{-4}$  [6, 4, 14]. Model validation was performed and good agreement was achieved [6]. However, it need to be realized, as generally found from the previous research in this area [13], that the difference between steady and unsteady simulation was expected and the unsteady simulation gave more accurate result than the steady one. It has revealed that the steady simulation (RANS) tends to predict less entropy generation than the experiment and unsteady (URANS) simulation [12-14]. However, this has to be trade off with computer resource and modeling complexity.

### 3.2 Boundary conditions and validations

- Inlet boundary condition; static frame, total pressure was assigned to 1 atm
- Outlet boundary condition; average static pressure was assigned to 4 atm
- Stationary Wall and no-slip condition was assigned to wall
- Inlet temperature was 30°C

The flow was modeled in steady flow regime. Air was treated as compressible.

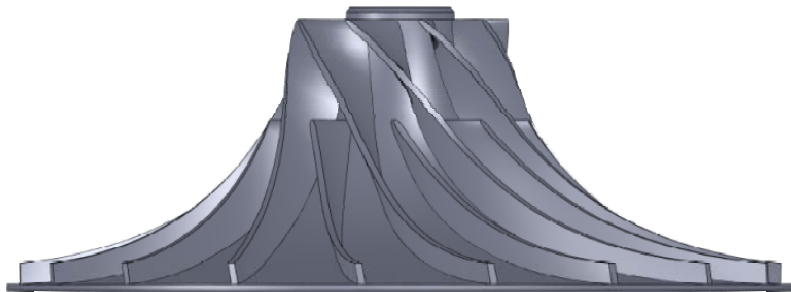


**Fig. 3.** Compressor geometry.

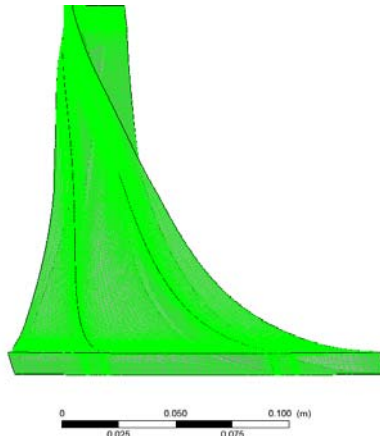


**Fig. 4.** Structure of hexahedral mesh.

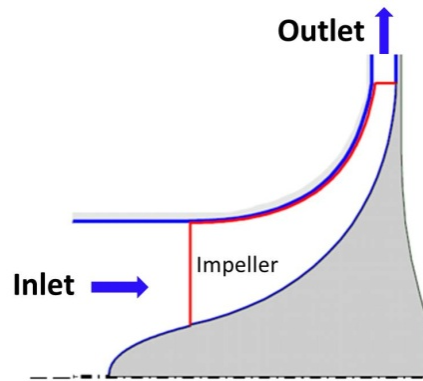


**Fig. 5.** Meridional plane of the computational domain.

Model validation had been done by comparing the simulation result from Rigi test rig at Turbomachinery Laboratory. ETH Zurich [6, 7] where the impeller model A8C41 (Albert Kammerer) was employed. Good agreement between testing result and simulation result was obtained.

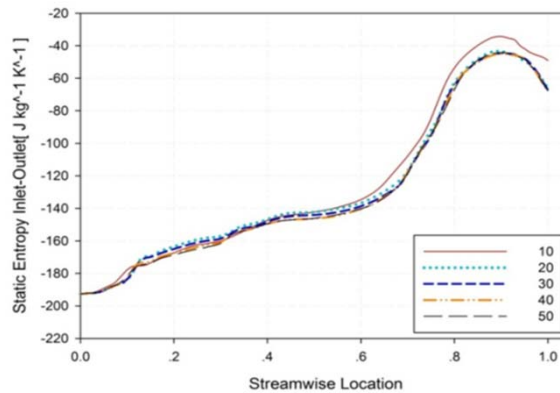


**Fig. 6.** Static entropy at different stream-wise location for all exit beta angle.

#### 4. RESULTS AND DISCUSSION

##### 4.1 Quantitative entropy generation

The simulation result showed the same character of entropy generation for all trailing edge blade angle ( $\beta_2$ ). The entropy generation was linearly increasing to around 60 J/kg-K at the stream-wise location range of 0-0.6, as shown

in Fig. 6. The total entropy generation at the stream-wise location range 0.6-1.0 was around 480 J/kg-K, which was 8 times more than that in the impeller inlet region. The highest total entropy generation was observed at the impeller exit region for the case of 10 degree exit beta angle. The lowest total entropy generation was revealed for the case of 50 degree exit beta angle. Nevertheless, back-flow occurred from recirculation at the exit computational domain, resulting in a decrease in entropy near the exit boundary cell faces. This was observed at 0.9 stream-wise location toward the exit of computation domain (Fig. 6).

#### 4.2 The influence of exit beta angle on secondary flow region

At stream-wise location range of 0-0.6, the flow was parallel to the flow passage (Figs. 11 and 12), because in-flow angle was coincide with the inlet impeller angle. The flow channel cross area was throated causing the fluid to accelerate along the flow passage (Fig. 7). It is easy to manage the flow in throat region since the flow momentum become higher along the passage. Flow separation is unlikely to occur in throat region. However, this was a trade-off with the flow blockage which limit the delivered mass flow rate of the compressor. Despite the separation was not observed in the impeller inlet area, the secondary flow was formed due to blade tip leakage that interacted with flow in the passage (Fig 8). Blade tip leakage was the cross-jet flow that induced secondary vortices within the flow passage.

It was difficult to manipulate the flow at the outlet area (0.6-1.0 stream-wise location). Since the flow was decelerated rapidly due to wider area passage, so called “diffuser”. Various physical interaction influenced flow field in this area. In general, Jet-wake region was formed (Figs. 13 and 14). Low pressure and low velocity zone in the suction side of the impeller blade was the cause of flow separation. This region tend to decelerated on some portion of the flow to separate from jet region. At the impeller outlet, jet-wake flow structure interacted with flow downstream resulting in recirculation flow at the impeller outlet (Figs. 13 and 14). Stronger secondary flow from blade tip leakage interaction, compared to the inlet region, could be observed.

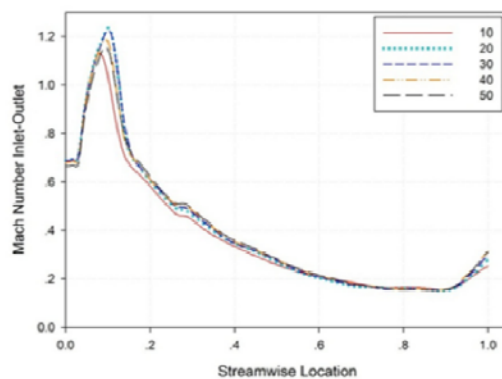


**Fig. 7.** Mach number at various stream wise locations for all exit beta angles.

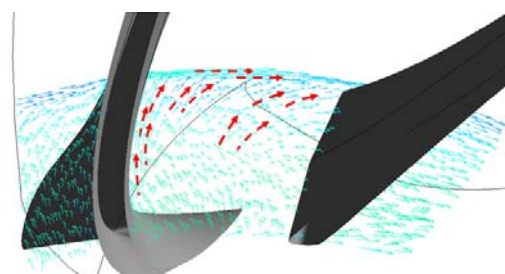


**Fig. 8.** Secondary flow at stream-wise location of 0.25.

Figs. 9 and 10, showed entropy generation along stream-wise location of the impeller blade. At the location range of 0.1-0.6, entropy generation was very little, resulting from non-deformation flow field at the inlet area as stated before. The major source of entropy generation came from near-wall region, which shear layer generated from both

secondary flow from blade leakage (Figs. 9 and 10) and boundary layer structure. At the location range of 0.5-0.7, more entropy was generated in near-wall region due to the development of boundary layer and blade tip leakage interaction. However, entropy generation was in the same level as the location 0-0.4 because of the flow in this location was diffused. It was around 400% lower in velocity magnitude compared to the location 0-0.4 (Fig. 7). At the location of 0.7-1.0, entropy generation was 3-4 times higher than of the location 0-0.6, because of the interaction of many physical phenomena that leading to high deformation flow field. The separation flow was formed in the region around 0.6 stream-wise location (Figs. 11 and 12), which was a beginning of the jet-wake flow structure. The accumulated secondary flow along blade tip and accumulated turbulence intensity that generated from local high shear flow structure was transported by convection mode from upstream flow to exit region of 0.7-1.0 location of the impeller.

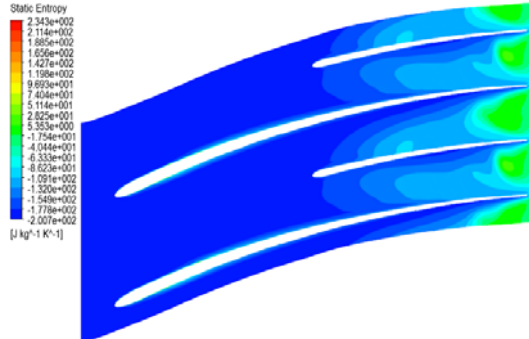


**Fig. 9.** Entropy distribution of case 10° exit beta angle.

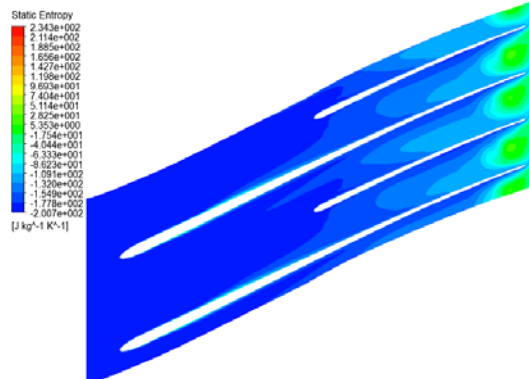


**Fig. 10.** Entropy distribution of case 50° exit beta angle.

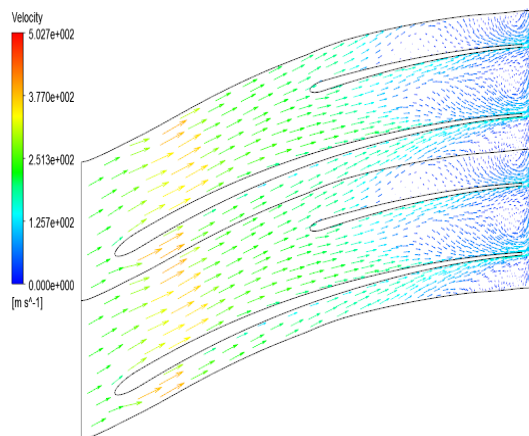


**Fig. 11.** Velocity structure of 10° exit beta angle.

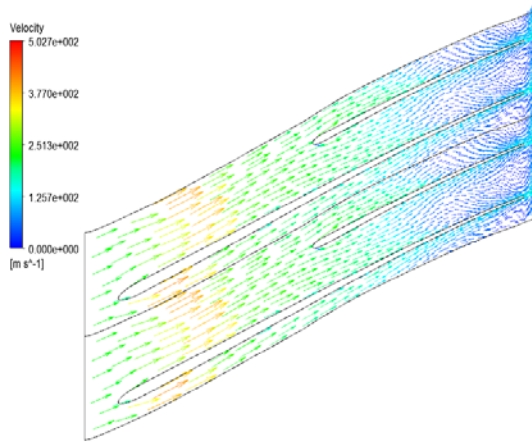


**Fig. 12.** Velocity structure of  $50^\circ$  exit beta angle.

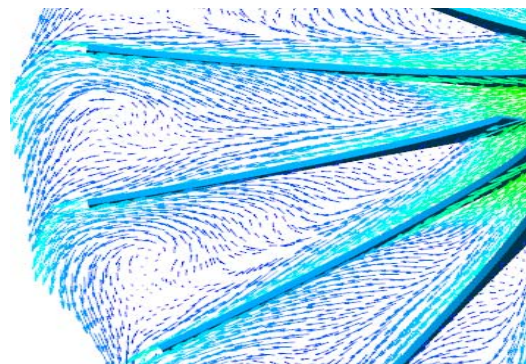


**Fig. 13.** Jet-wake and recirculation structure of  $10^\circ$  exit beta angle.

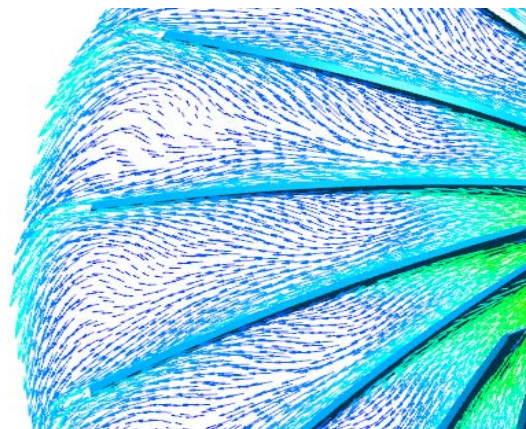


**Fig. 14.** Jet-wake and recirculation structure of  $50^\circ$  exit beta angle.

Beta angle has a significant impact on flow structure. By increasing it the Jet-wake shear layer structure could be alleviated. The flow was accelerated in a low-momentum wake region by increasing beta angle as a result of smaller flow cross sectional area (Fig. 17)

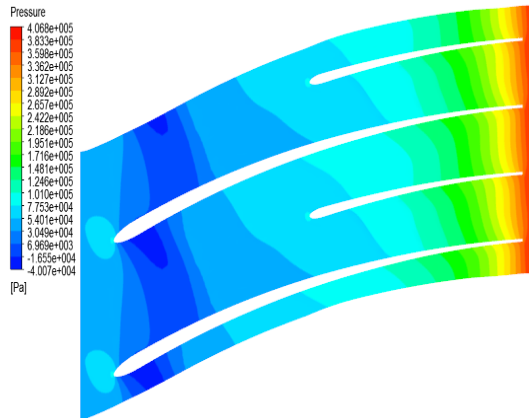


**Fig. 15.** Pressure distribution of 10° exit beta angle.

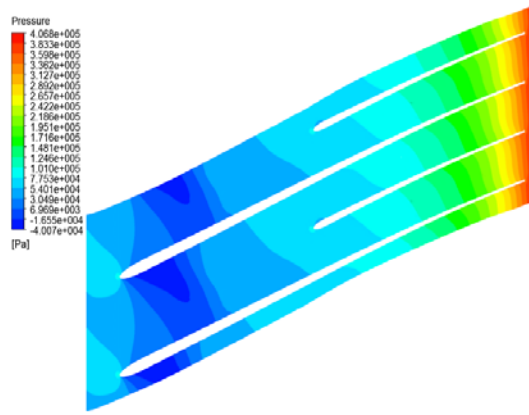


**Fig. 16.** Pressure distribution of 50° exit beta angle.

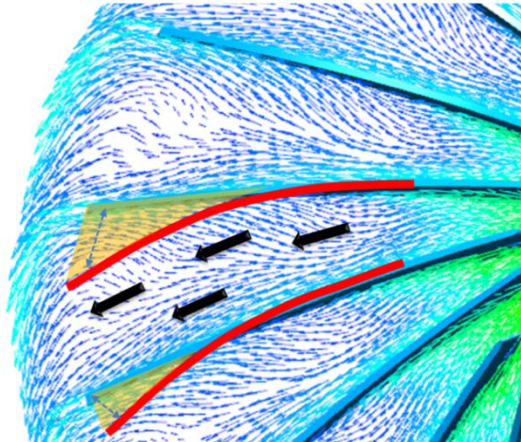


**Fig. 17.** Effect of beta angle that cause smaller area in wake region and wider area in jet region.

## 5. CONCLUSION

A computational investigation has been undertaken to investigate on the characteristic of entropy generation along blade passage of the centrifugal compressors. The impeller exit beta angle influenced on the entropy generation and flow field, is depicted. Four different exit beta angle values provided same entropy generation characteristic. At stream-wise location of 0.1-0.6, the entropy generation is almost the same for all four cases, which is very little comparing to impeller exit region. At the impeller exit region (0.6-1.0 stream-wise), massive entropy generation

was formed. Because there are several physical interaction in this area. The exit beta angle has influenced on the impeller outlet flow pattern resulting in less entropy generated, compared to inlet region. The lowest entropy generation was observed in the case of beta angle 50°. The highest entropy generation occur in the case of beta angle 10°. Flow field velocity showed that exit beta angle effect on the flow structure in exit area. Beta angle alleviated on the jet-wake shear layer and also impeller exit flow distortion. The separation flow was earlier found in the case of low Beta angle. Higher deformation rate of flow structure can be observed in the case of low beta angle.

## REFERENCES

- [1] Soares, C. *Microturbines Application for Distributed Energy System*, London, Elsevier, 2007.
- [2] Anish, S. and Sitaram, N. Computational investigation of impeller-diffuser interaction in a centrifugal compressor with different types of diffusers, *Proceedings of the Institution of Mechanical Engineers, Part A: Journal of Power and Energy*, Vol. 223, 2009, pp. 167-178
- [3] Liu, R. and Xu, Z. Numerical investigation of a high-speed centrifugal compressor with hub vane diffusers, *Proceedings of the Institution of Mechanical Engineers, Part A: Journal of Power and Energy*, Vol. 218(3), 2004, pp. 155-169, 2004, pp. 155-169.
- [4] Wilson, D.G. *The Design of High-Efficiency Turbomachinery and Gas Turbines*, Cambridge, MA: The MIT Press, 1984.
- [5] Asuaje, M., Bakir, F., Smaine, K. and Rey, R. Inverse design method for centrifugal impellers and comparison with numerical simulation tools, *International Journal of Computational Fluid Dynamics*, Vol. 18(2), 2004, pp. 101-110.
- [6] Armin, Z., Albert, K. and Abhari, R.S. Unsteady Computational Fluid Dynamics investigation on inlet distortion in a centrifugal compressor. *Journal of Turbomachinery*, Vol. 132, 2010, paper number 031015 (9 pages)
- [7] Schleer, M. and Abhari, R.S. Clearance effects on the evolution of the flow in the vaneless diffuser of a centrifugal compressor at part load condition, *Journal of Turbomachinery*, Vol. 130, 2008, paper number 031009 (9 pages).
- [8] Tang, J., Turunen-Saaresti, T. and Lorjola, J. Use of partially shrouded impeller in a small centrifugal compressor. *Journal of Thermal Science*, Vol. 17, 2008, pp. 21-27.
- [9] Baskharone, E.A. *Principle of Turbomachinery in Air-Breathing Engines*, Cambridge University, New York, Cambridge University Press, 2006.
- [10] Dixon, S.L. (2005). *Fluid mechanics and thermodynamics of turbomachinery*, Liverpool, Butterworth-Heinemann.
- [11] Florin, L., Trevino, J. and Sommer, S. Numerical Analysis of Blade Geometry Generation Techniques for Centrifugal Compressors. *International Journal of Rotating Machinery*, 2007.
- [12] Trébinjac, I., Kulisa, P., Bulot, N. and Rochuon, N. Effect of Unsteadiness on the Performance of a Transonic Centrifugal Compressor Stage. *Journal of Turbomachinery*, Vol. 131, 2009, paper number 041011 (9 pages)
- [13] Dickmann, H.P., Wimmel, T.S., Szwedowicz, J., Filsinger, D., and Roduner, C.H. Unsteady flow in a turbocharger centrifugal compressor: Three-dimensional computational fluid dynamics simulation and numerical and experimental analysis of impeller blade vibration, *Journal of Turbomachinery*, Vol. 128, 2006, pp. 455-465.
- [14] Pierandreiand, G. and Sciubba, E. Numerical Simulation and Entropy Generation Maps of an Ultra-Micro-Turbogas Compressor Rotor. ECOS 2010, 14-17 June 2010, Lausanne CH, 2010.
- [15] ANSYS CFX-Solver Theory Guide. ANSYS CFX Release 12.1, ANSYS Europe Ltd., 1996-2006.